

Collagen density regulates tip–stalk cell rearrangement during angiogenesis via cellular bioenergetics

Cite as: APL Bioeng. **8**, 026120 (2024); doi:10.1063/5.0195249

Submitted: 1 January 2024 · Accepted: 7 May 2024 ·

Published Online: 10 June 2024













View Online



Export Citation



CrossMark

Wenjun Wang,¹  Matthew R. Zanotelli,^{1,2}  Lindsey N. Sabo,¹  Emily D. Fabiano,¹  Natalie M. Goldfield,¹ 
Chloe Le,³  Elle P. Techasiriwan,¹  Santiago Lopez,¹  Emily D. Berestesky,¹ 
and Cynthia A. Reinhart-King^{1,a)} 

AFFILIATIONS

¹Department of Biomedical Engineering, Vanderbilt University, Nashville, Tennessee 37235, USA

²Nancy E. and Peter C. Meinig School of Biomedical Engineering, Cornell University, Ithaca, New York 14853, USA

³Department of Biological Sciences, Vanderbilt University, Nashville, Tennessee 37235, USA

Note: This paper is part of the special issue on Physical Sciences Approaches to Cancer Research.

^{a)}Author to whom correspondence should be addressed: cynthia.reinhart-king@vanderbilt.edu. Tel. 615-875-8309

ABSTRACT

Tumor vasculature plays a crucial role in tumor progression, affecting nutrition and oxygen transportation as well as the efficiency of drug delivery. While targeting pro-angiogenic growth factors has been a significant focus for treating tumor angiogenesis, recent studies indicate that metabolism also plays a role in regulating endothelial cell behavior. Like cancer cells, tumor endothelial cells undergo metabolic changes that regulate rearrangement for tip cell position during angiogenesis. Our previous studies have shown that altered mechanical properties of the collagen matrix regulate angiogenesis and can promote a tumor vasculature phenotype. Here, we examine the effect of collagen density on endothelial cell tip–stalk cell rearrangement and cellular energetics during angiogenic sprouting. We find that increased collagen density leads to an elevated energy state and an increased rate of tip–stalk cell switching, which is correlated with the energy state of the cells. Tip cells exhibit higher glucose uptake than stalk cells, and inhibition of glucose uptake revealed that invading sprouts rely on glucose to meet elevated energy requirements for invasion in dense matrices. This work helps to elucidate the complex interplay between the mechanical microenvironment and the endothelial cell metabolic status during angiogenesis, which could have important implications for developing new anti-cancer therapies.

© 2024 Author(s). All article content, except where otherwise noted, is licensed under a Creative Commons Attribution-NonCommercial 4.0 International (CC BY-NC) license (<https://creativecommons.org/licenses/by-nc/4.0/>). <https://doi.org/10.1063/5.0195249>

INTRODUCTION

Angiogenesis is a process in which new blood vessels form via sprouting from existing vessels.¹ During angiogenesis, endothelial cells proliferate, migrate into the surrounding stroma, and arrange themselves into spouts. As the cell spouts get longer, the newly formed endothelium differentiates into tip and stalk cells, and tip cells then coordinate with stalk cells to elongate the sprout.² Maintaining an appropriate tip–stalk cell dynamic is critical for regulating sprouting during angiogenesis.³ In healthy tissue, the microenvironment regulates angiogenesis by tightly controlled chemical and mechanical cues that typically maintain quiescence.^{4,5} However, the tight regulation of angiogenesis is lost during tumor progression, resulting in an increased activation of angiogenesis that disrupts the tight regulation of blood vessel formation and results in abnormal tumor vasculature.⁶ Solid

tumor vasculature is characterized by leaky, tortuous, disorganized, and misshapen blood vessels that create heterogeneous blood flow and elevated interstitial pressure that collectively contribute to tumor progression and a more aggressive phenotype.^{6–8} Thus, many studies have sought to increase the effectiveness of tumor treatments via normalizing tumor vasculature.^{7,8}

Angiogenesis relies on the coordinated behavior of highly migratory tip cells at the front of new sprouts and quiescent stalk cells that trail and elongate the sprout. However, tip and stalk cells are not genetically predetermined, and angiogenic sprouting is a dynamic process where endothelial cells actively rearrange and switch tip position to allow more competitive stalk cells to overtake the lead, with rearrangement requiring energy-intensive actin remodeling and traction force generation.^{9,10} Given the high energy requirements for angiogenic

sprouting and invasion, metabolism has been shown to play a crucial role in controlling tip vs stalk cell specification during angiogenic invasion and has been implicated as a driver of the angiogenic switch.¹¹ Tumor endothelial cells, like cancer cells, exhibit an increased rate of glycolysis, and recent studies have shown that targeting tumor endothelial cell glycolysis has the potential to induce vascular normalization.¹² As such, there is growing interest in targeting endothelial cell metabolism to inhibit angiogenesis.

While tissue mechanics have a prominent role in angiogenesis and tumor angiogenesis, and increased collagen cross-linking alone can induce a tumor vasculature phenotype,¹³ the impact of the tumor microenvironment's physical properties on metabolism is often underestimated. Here, we explored the effect of collagen density on tip–stalk cell dynamics during angiogenic sprouting and monitored the energy dynamics of sprouting endothelial cells utilizing a genetically engineered fluorescent biosensor of intracellular ATP:ADP ratio. Our data indicate that the tip–stalk cell switching rate and the energy difference between the tip and stalk cells increased with collagen density. We identify a correlation between the cells' energy state, spatial positioning, and the rearrangement of tip cells, indicating angiogenesis through dense collagen is more energetically demanding than angiogenesis in less dense collagen. These insights link the mechanics of the cellular matrix, cellular metabolism, and tumor endothelial cell behavior during angiogenic sprout formation and outgrowth.

RESULTS

Increased collagen density reduces invasion and increases energy levels of angiogenic sprouts

To examine the impact of collagen density on angiogenic sprouting, we used a three-dimensional *in vitro* spheroid-based angiogenesis

assay, which gives rise to capillary-like sprouts that mimic the physiological arrangement of endothelial cells in vessels.^{14–16} Here, we examined 3–7 mg/ml type I collagen matrices, which show decreasing pore size and fiber length with increasing collagen density [Figs. 1(a) and 1(c)]. Human umbilical endothelial cell (HUVEC) spheroids were embedded in collagen gels and cultured for 72 h, and the collective invasion of multicellular sprouts into the surrounding collagen matrix was assessed. Immunofluorescent labeling of angiogenic sprouts with the endothelial cell marker CD31 and phalloidin showed that collagen density had a significant impact on spheroid outgrowth. In high-density collagen with a more confined and difficult to migrate microenvironment, spheroid sprout length and the number of sprouts per spheroid also decreased, indicating that spheroid invasion was reduced [Figs. 1(d) and 1(f)].

Given that angiogenic sprouting is an energy-demanding process and heightened collagen density inhibited sprouting, we next examined how a cellular energetic level responds to collagen density.^{11,17} HUVECs were transduced with fluorescent intracellular ATP:ADP biosensor PercevalHR, enabling measurements of cellular energetics.¹⁸ We have previously shown that collagen density impacts the cellular energetics of individual and collectively migrating cells and that the ATP:ADP ratio correlates with energy utilization.^{19–22} To examine endothelial cell energetics during angiogenic sprouting, HUVEC spheroids expressing PercevalHR were embedded in collagen matrices of different densities and the intracellular ATP:ADP ratio was measured after 72 h. HUVEC spheroids in high-density collagen matrices exhibited increased intracellular ATP:ADP ratio in invading angiogenic sprouts [Figs. 2(a) and 2(b)]. Changes in migration were significantly correlated with cellular energetics, with sprouts in matrix conditions most permissive to invasion having lower ATP:ADP ratios [Fig. 2(c)]. Together, these results indicate that endothelial cell invasion through dense collagen during angiogenic sprouting consumes high amounts

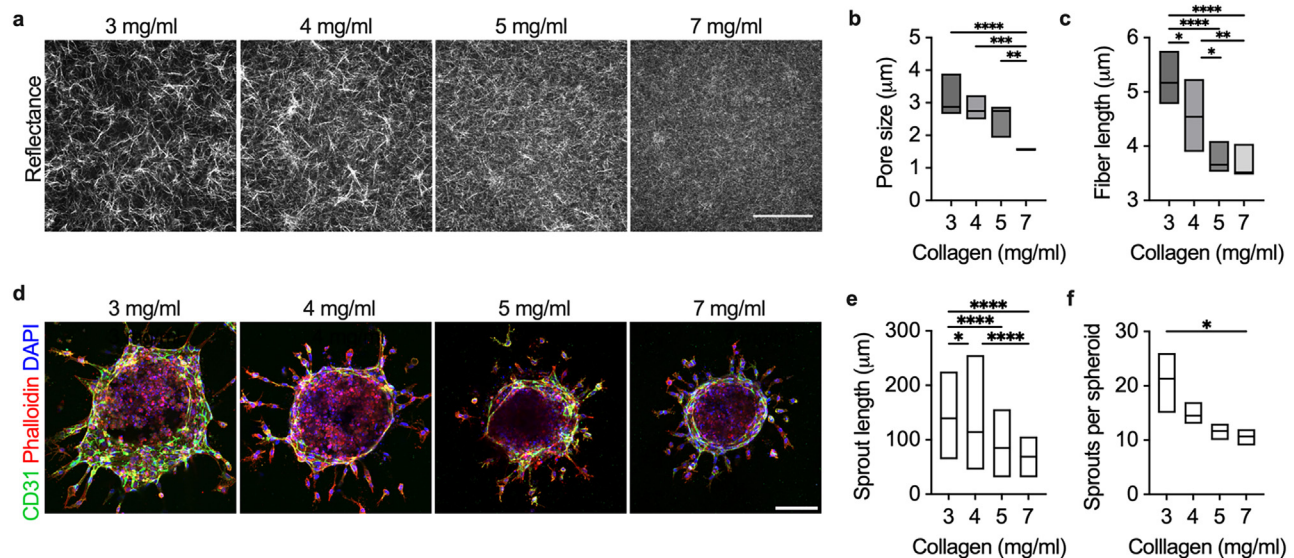
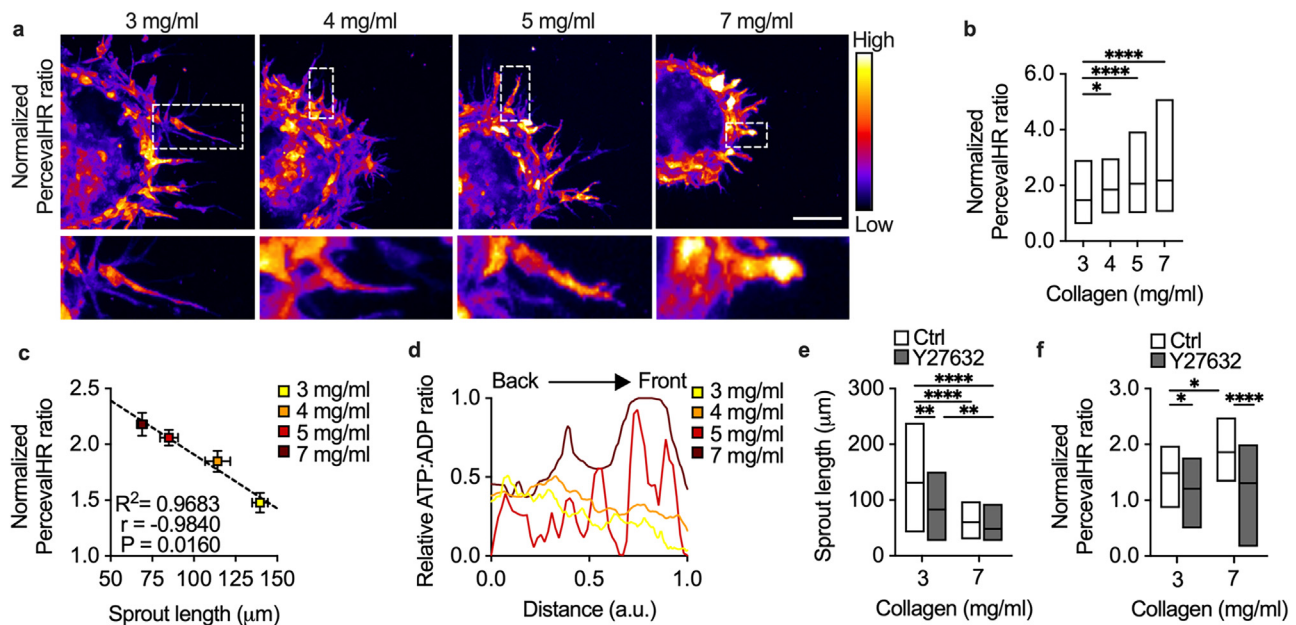


FIG. 1. Increased collagen density reduces invasion of angiogenic sprouts. (a) Representative images of confocal reflectance visualizing collagen architecture. (b) and (c) Quantification of pore size (b) and fiber length (c) of collagen matrices ($n = 5$). (d) Representative images of HUVEC spheroids embedded in collagen matrix with different densities. Samples were stained for actin and DAPI to visualize the outgrowths. (e) and (f) Quantification of (e) sprout length and (f) the number of sprouts per spheroid ($n = 60, 37, 32,$ and 34 for $3, 4, 5,$ and 7 mg/ml collagen, respectively). Data are presented as floating bars (min to max) with the line at the mean value. * $P < 0.05$, ** $P < 0.01$, *** $P < 0.001$, and **** $P < 0.0001$; scale bar = $100 \mu\text{m}$.



of cellular energy, potentially due to the denser matrix requiring more energy for invasion.

The energy levels of angiogenic sprouts are correlated with invasion and cell contractility

Successful invasion requires cells to respond to the physical cues in the surrounding matrix utilizing actomyosin contractility to coordinate mechanosensing,²³ with cell contractility increasing with increasing collagen density.²⁴ The ATP:ADP ratio was elevated at the forefront of invading strands, suggesting cells at the forefront of invading sprouts, where highly motile tip cells are located, were using more energy [Fig. 2(d)]. Interestingly, the leading edge is also where filopodia and actin-containing protrusive structures interact and remodel the matrix,^{25,26} with invasion into dense matrices triggering high filopodia density.

Therefore, we examined the impact of cell contractility on spheroid invasion and angiogenic sprout energetics by treating spheroids with the ROCK inhibitor Y27632 to block cell contractility. Indeed, the inhibition of cell contractility following treatment with Y27632 not only decreased spheroid invasion but also decreased the high ATP:ADP ratio of angiogenic sprouts in 7 mg/ml collagen [Figs. 2(e) and 2(f)]. These findings suggest that collagen density-mediated cell contractility during invasion is associated with increased bioenergetics in dense collagen.

Tip-stalk cell switching rate during angiogenic sprouting is accelerated in dense collagen

Cellular competition between tip and stalk cells significantly influences the iterative sprouting processes in angiogenesis,⁹ and while

collagen density has been shown to restrict angiogenesis,¹³ the influence of the physical microenvironment on endothelial cell competition has largely not been explored. To examine the effects of matrix cues on tip cell rearrangement during angiogenic sprouting, HUVEC spheroids were labeled with the far-red fluorescent nuclear DNA stain DRAQ5 and cultured in 3 – 7 mg/ml collagen matrices for 72 h, then the cell position during invasion was examined over 18 h [Fig. 3(a), supplementary material video S1–S4]. HUVEC spheroids collectively invaded the surrounding collagen, during which cells dynamically shuffled tip position within strands [Figs. 3(a) and 3(b)]. Notably, the lifetime of tip cells reduced with increasing collagen density, as angiogenic sprouts in dense matrices required more cell rearrangement during invasion [Fig. 3(c)]. The tip–stalk cell switching rate was dependent on cell contractility, as Y27632 treatment reduced invasion and the cell lifetime at the tip position [Fig. 3(d)]. These observations suggest that denser matrices necessitate more extensive cell rearrangement for effective invasion.

Tip cells uptake more glucose to invade through dense collagen

Glucose is a main source of cellular energy production and has been associated with invasiveness,²⁷ with cells collectively moving toward a glucose gradient to reduce the energy cost of migration.²⁸ Given our results indicate collagen density increases the cellular energy state of invading sprouts, we investigated if altered glucose uptake could account for the change in intracellular ATP:ADP with collagen density. To measure glucose uptake *in vitro*, we used the fluorescent glucose analog, 2-NBDG. After 72 h of culture in collagen gels,

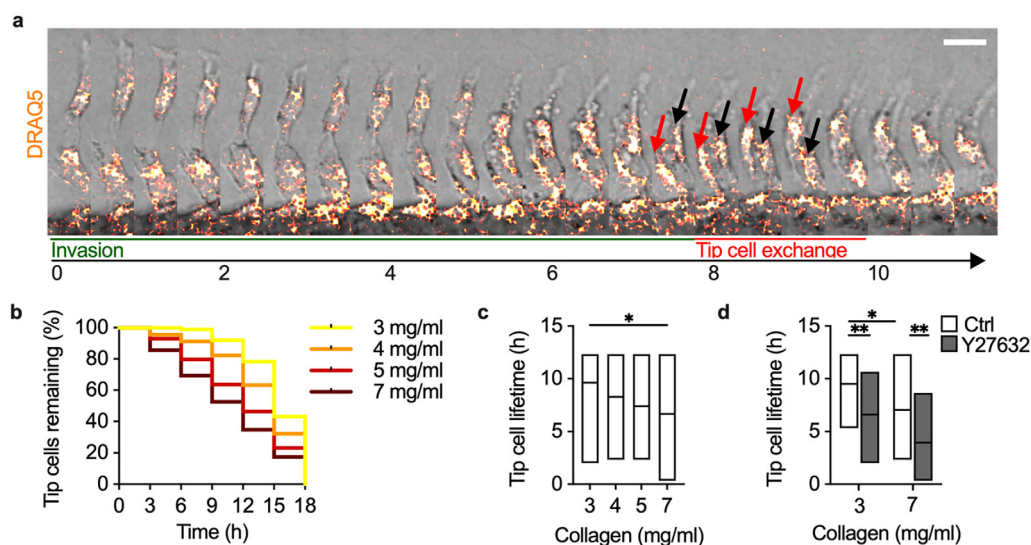


FIG. 3. Collagen density affects tip–stalk cell rearrangement in angiogenic sprouts. (a) Representative images of HUVEC spheroids labeled with DRAQ5. Angiogenic sprouting was tracked over time. (b) The number of cells remaining at the tip position of angiogenic sprouts decreases with increasing collagen density. (c) Quantification of time spent at the tip position before being overtaken by a stalk cell decreases as density increases ($n = 31, 19, 13, 8$ cells for 3, 4, 5, and 7 mg/ml collagen, respectively). (d) Quantification of tip cell lifetime following Y27632 treatment. Data are presented as floating bars (min to max) with the line at the mean value. * $P < 0.05$ and ** $P < 0.01$; scale bar = 25 μm .

HUVEC spheroids were incubated with 2-NBDG for 24 h, and glucose uptake was quantified. While the bulk GLUT1 expression level of cells embedded in 3 mg/ml and 7 mg/ml gel was similar (supplementary material Fig. S1), we observed increased glucose uptake in more dense collagen gels [Figs. 4(a) and 4(b)]. To elucidate the connection between the glucose uptake of endothelial cells and their cellular position within invading angiogenic sprouts, we quantified the glucose uptake of tip and stalk cells, respectively, using 2-NBDG to assess intracellular glucose concentrations. HUVEC spheroids were cultured for 72 h in collagen gels, followed by a 24 h incubation with 2-NBDG, and then spheroids were fixed and imaged to evaluate glucose uptake. To delineate cell boundaries and identify tip vs stalk cells in sprouts, spheroids were stained with WGA to label cell membranes. We observed a significantly higher glucose uptake in tip cells compared to stalk cells, a disparity that intensified with the increase in collagen density [Figs. 4(c) and 4(e)]. Matrix densities that exhibited a more significant differential in glucose uptake between tip and stalk cells (2-NBDG tip:stalk) corresponded with a reduced tip cell lifetime [Fig. 4(f)]. These results suggest that dense matrices present a more significant challenge for cell invasion, necessitating increased cell energy expenditure and increased switching between tip and stalk cells. Specifically, tip cells require higher energetic costs than stalk cells during angiogenic sprouting, likely resulting in the stalk cells replacing the tip cell to maintain outgrowth in challenging and energetically demanding microenvironments.

Glucose uptake is associated with invasion, cellular energetics, and tip–stalk cell switching

To assay the effects of inhibition of metabolism on the invasion and energy state of angiogenic sprouts, we embedded HUVEC spheroids in collagen matrices and treated cells with BAY876, a GLUT1

inhibitor that blocks glucose transportation. Here, we investigated the requirement of glucose uptake in supporting the increased energy state and tip cell switching rate of invading sprouts in high-density collagen. HUVEC spheroids were embedded in collagen matrices, grown for 72 h, then treated with the GLUT1 inhibitor, BAY876. Using quantitative polarization microscopy to measure cell contractility in three-dimensional matrices, we found that GLUT1 inhibition significantly lowered the contractility of invading sprouts in both 3 and 7 mg/ml collagen, and spheroids exhibited lowered outgrowth [Figs. 5(a) and 5(c)]. We next examined the impact of glucose uptake inhibition on cellular energy state. BAY876 treatment lowered glucose uptake, as expected, and lowered the ATP:ADP ratio, such that there was no longer a significant difference between sprouts in 3 and 7 mg/ml collagen [Fig. 5(d)]. Notably, the inhibition of GLUT1 also significantly decreased tip cell lifetime [Fig. 5(e)]. Together, these results indicate that glucose uptake supports the elevated energy state of angiogenic sprouts in dense collagen matrices, and glucose uptake is required to maintain tip cell invasion.

DISCUSSION

The mechanical properties of tumor stroma play a crucial role in modulating cell functions, with emerging evidence linking matrix mechanics and metabolism to cell migration.^{19–22} Our study indicates that increased collagen density accelerates the rate of tip–stalk cell switching during angiogenesis, which is correlated with the energy state of the cells. These findings highlight how the physical cues in the microenvironment influence endothelial cell metabolism and suggest that tip–stalk cell switching is related to the metabolic costs of tip cell invasion. Our research uncovers a complex interaction between the mechanical characteristics of the extracellular matrix (ECM), endothelial cell metabolism, and tip–stalk cell rearrangement in angiogenesis.

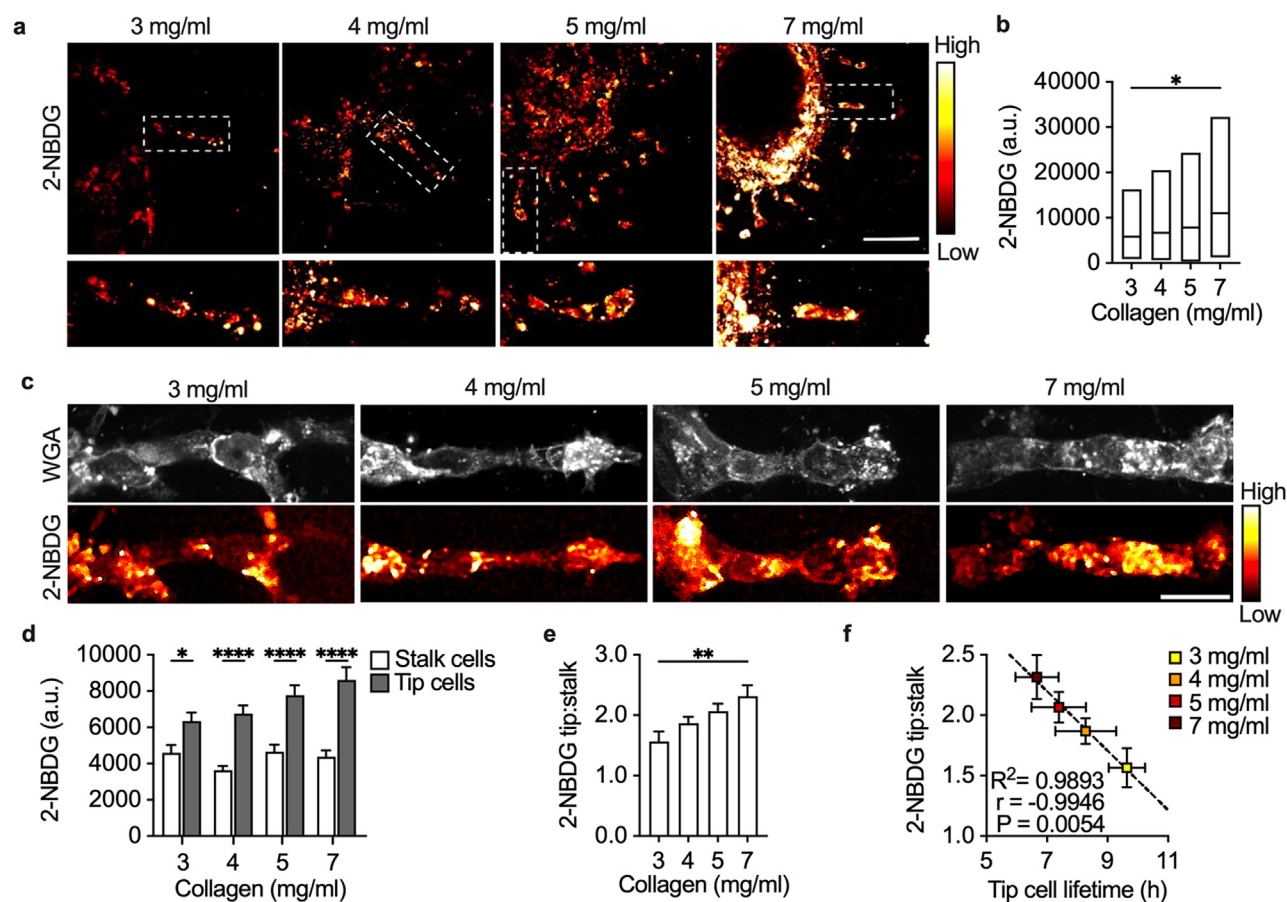


FIG. 4. Collagen density alters tip-stalk cell glucose uptake. (a) and (b) Representative heatmap and quantification of intracellular 2-NBDG level in invading angiogenic sprouts for HUVEC spheroids in varying collagen densities ($n = 36, 37, 78,$ and 48 for $3, 4, 5,$ and 7 mg/ml collagen, respectively). (c) Representative heatmap and WGA staining of the intracellular 2-NBDG level in tip and stalk cells of invading angiogenic sprouts. (d) Quantification of 2-NBDG uptake in tip vs stalk cells across varying collagen densities. (e) Ratio of glucose uptake between tip and stalk cells within spheroids embedded in collagen with different densities. (f) Relationship between tip-stalk cell glucose uptake and tip cell lifetime across collagen densities ($n = 28, 59, 41,$ and 28 cells for $3, 4, 5,$ and 7 mg/ml, respectively). Data are presented as floating bars (min to max) with the line at the mean value. * $P < 0.05,$ ** $P < 0.01,$ and **** $P < 0.0001;$ scale bar = 100 (a) and $20 \mu\text{m}$ (c).

Together, this work identifies mechanical mechanisms that may contribute toward aberrant metabolism found in tumor endothelial cells and promote abnormal tumor vasculature.

Migration costs substantial energy, and localized energy production is essential to support cytoskeletal remodeling and the formation of protrusions at the forefront of migrating cells.^{29,30} Our findings that suggest migration is energy intensive are supported by prior work demonstrating that the architecture and mechanical properties of the ECM affect cancer cellular energy use during migration, influencing the choice of migration paths.^{19,20} Breast cancer cells increase energy consumption during invasion in denser collagen matrices during both single-cell and collective migration.^{20,22} Leading cells at an invasive front have also been shown to dynamically change based on metabolic costs.^{7,8,22,28} During collective migration, the invasion process is governed by the energy states of leader and follower cells, where a follower cell takes the lead after a leader cell exhausts its energy to ensure continuous migration.²² Like a leader cell during collective migration that bears most of the energetic load during invasion, the tip cell of an

angiogenic stalk bears most of the energetic load of vessel outgrowth. Consequently, increased energy costs associated with moving through a dense matrix might significantly affect the frequency of cell shuffling and angiogenesis.³¹ While we characterized how collagen density-mediated physical cues within the local microenvironment regulate cell energetic status and tip-stalk cell switching of endothelial cells, we are aware that collagen with different densities may provide various amounts of adhesion sites and biochemical microenvironment to cells. Further studies would be needed to tease apart the influence of biochemical microenvironments and mechanical properties on endothelial angiogenic behaviors.

Endothelial tip cells, characterized by their high motility and extensive filopodia formation during migration, demand significant energy.³² By tracking the migration of individual endothelial cells invading strands of HUVEC spheroids, our study revealed a dynamic reorganization of tip cells and stalk cells during angiogenic sprouting, which was correlated with cellular energy status. We observed that the frequency of tip-stalk cell turnover increases with collagen density.

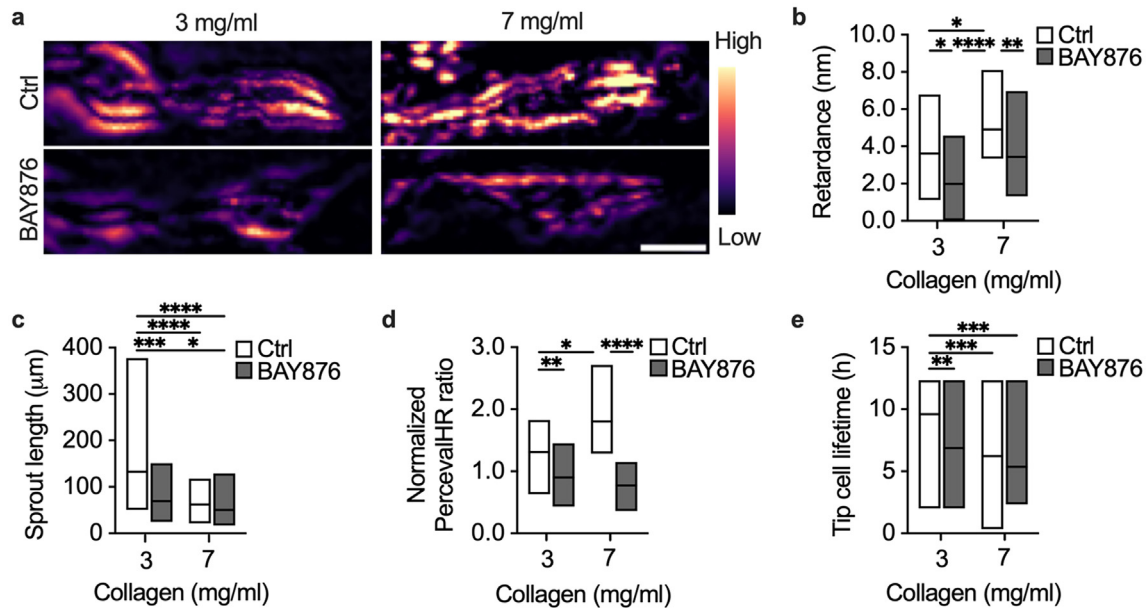


FIG. 5. Glucose uptake inhibition lowers contractility, cell energy state, and tip-stalk cell switching of angiogenic sprouts. (a) Representative heatmap images of retardance of angiogenic sprouts. (b) Average retardance of sprouts showing the cell contractility of sprouts ($n = 20$ for 3 mg/ml Ctrl, $n = 18$ for 3 mg/ml BAY876, $n = 26$ for 7 mg/ml Ctrl, and $n = 31$ for 7 mg/ml BAY876). (c) Quantification of sprout length of HUVEC spheroids embedded in collagen with 3 or 7 mg/ml collagen treated with or without BAY876 ($n = 32$ for 3 mg/ml Ctrl, $n = 40$ for 3 mg/ml BAY876, $n = 36$ for 7 mg/ml Ctrl, and $n = 42$ for 7 mg/ml BAY876). (d) Quantification of normalized ATP:ADP ratio of angiogenic sprouts ($n = 25$ for 3 mg/ml Ctrl, $n = 28$ for 3 mg/ml BAY876, $n = 23$ for 7 mg/ml Ctrl, and $n = 16$ for 7 mg/ml BAY876). (e) Quantification of tip cell lifetime following BAY876 treatment ($n = 25$ for 3 mg/ml Ctrl, $n = 28$ for 3 mg/ml BAY876, $n = 23$ for 7 mg/ml Ctrl, and $n = 16$ for 7 mg/ml BAY876). Data are presented as floating bars (min to max) with the line at the mean value. * $P < 0.05$, ** $P < 0.01$, *** $P < 0.001$, and **** $P < 0.0001$.

Inhibition of glucose uptake lowered the energy state of angiogenic sprouts in dense collagen matrices, and decreased the cell contractility and frequency of tip-stalk cell switching within angiogenic sprouts. Tip-stalk cell switching likely sustains invasion despite the energetic costs of sprout outgrowth, which could in part explain why the rate of switching increases in denser collagen. Interestingly, the roles of tip and stalk cells are not fixed by genetics, but rather exhibit plasticity with reversible phenotypes.¹⁰ Therefore, excessive shuffling during sprouting could disrupt developing the proper pattern of tip and stalk cells, interfering with proper branching, and potentially leading to abnormal angiogenesis. Excessive tip cell behavior has been shown to lead to excess branching and denser vascular networks, common in tumor vasculature.³³ Our work raises the question of whether branching helps to minimize the energetic impact to a cell by identifying less energetically demanding paths, which will be addressed in future work.

Tumor endothelial cells display similar metabolic characteristics to cancer cells, favoring hyperglycolytic metabolism.¹² Activation of glycolytic activator PFKFB3 significantly impacts cell dynamics during angiogenesis, leading to the aberrant tumor vasculature. Blockage of endothelial PFKFB3 promotes tumor vessel normalization, which suggests that interruption of metabolic pathways is a promising strategy for vascular normalization.^{34–36} While many studies have ventured into normalizing tumor vasculature via suppression of specific signaling molecules, such strategies frequently encounter challenges due to the emergence of cellular escape mechanisms.^{37,38} For example, the initial response to anti-angiogenic therapies targeting the VEGF pathway

is always followed by a restoration of tumor progression.³⁹ The development of innovative approaches for normalizing tumor vasculature may be a key step in developing more effective cancer treatments. Recent findings suggest that targeting mechanical cues within tumors or mechanosensing pathways could be a viable strategy. Emerging evidence now highlights the significant role of metabolism in this context.^{35,40} These insights highlight the influence of ECM on angiogenesis through cellular energy dynamics, suggesting that manipulating ECM-mediated cellular energy states and metabolism could offer new avenues for cancer therapy and the normalization of tumor vasculature.

CONCLUSION

Previous research has established that the density of the collagen matrix is a critical factor in regulating angiogenesis and cell migration. Like cancer cells, endothelial cells undergo metabolic shifts and experience tip-stalk cell dynamics during invasion. However, the intricate relationship between collagen density, cellular metabolism, and the dynamics of tip-stalk cell rearrangement remains less explored. In our study, we employed the PercevalHR probe alongside the 2-NBDG glucose uptake assay to measure the metabolic status of endothelial cells during angiogenesis. Additionally, we used time-lapse imaging to track the tip-stalk cell rearrangement during angiogenic invasion. We found that increased collagen density impedes invasion and leads to a higher frequency of tip position changes. Notably, this increased rate of tip-stalk switching correlates with the energetic state of the cells suggesting

that the switching occurs in response to intracellular energetic state. This research highlights the pivotal role of cellular energy status in regulating mechanical properties of tip–stalk cell rearrangement during angiogenesis. Furthermore, our study sheds light on the mechanical signals within the tumor microenvironment that contribute to altered metabolism in endothelial cells, ultimately influencing the abnormal phenotype of tumor vasculature.

METHODS

Cell culture and reagents

Human umbilical vein endothelial cells (HUVECs; Lonza, Basel, Switzerland) were maintained in endothelial growth medium 2 (EGM-2; Lonza) at 37 °C and 5% CO₂. Only cells between passages 3 and 5 were used in experiments. To quantify the energetic status of cells, FUGW-PercevalHR (#49083, Addgene) and GW1-pHRed (#31473, Addgene) were transduced and co-expressed in the HUVECs via lentivirus in the presence of 8 μg/ml polybrene (Santa Cruz Biotechnology). To produce lentivirus, HEK-293T cells (CRL-3216, ATCC) were transfected with lentiviral FUGW-PercevalHR or GW1-pHRed together with second-generation packing constructs psPAX2 (Addgene) and pMD2.G (Addgene) in TransIT-LT1 (Mirus). Lentiviral particles were harvested 48 and 72 h post-transfection and then concentrated with a Lenti-X Concentrator (Takara Bio). To inhibit the Rho-kinase (ROCK), cells were treated with Y27632 (Millipore Sigma) at 10 μM concentration.⁴¹ To inhibit glucose uptake, HUVECs were treated with BAY876 (Millipore Sigma, Burlington, MA, USA), a GLUT1 inhibitor at 100 nM concentration.⁴² All cell lines were tested and found negative for mycoplasma contamination using the Universal Mycoplasma Detection Kit (30-1012K, ATCC).

Spheroid generation and embedding

HUVEC spheroids were prepared as described previously.¹³ Briefly, HUVECs were suspended in EGM-2 supplemented with 0.25% MethoCult (STEMCELL Technologies) and then plated into 96-well round-bottom plates (Costar, Corning Inc) at 10 000 cells per well. Plates were centrifuged at 1000 rpm for 5 min and cultured for 48–72 h at 37 °C and 5% CO₂ to allow spheroid formation. After spheroids formed, they were encapsulated in collagen matrices with 3, 4, 5, and 7 mg/ml density. 10 mg/ml type I collagen stock solution was diluted in 0.1% sterile acetic acid, then mixed with spheroid suspension and 10× PBS, HEPES, and neutralized with sodium bicarbonate to form 300 μl collagen gels with 1× PBS, 25 mM HEPES, and 44 mM sodium. Each collagen gel was embedded with 2–3 HUVEC spheroids and incubated at 37 °C and 5% CO₂ for 1 h to polymerize. After polymerization, cells were fed with 500 μl EGM-2 per well and cultured at 37 °C and 5% CO₂ until experiments.

Quantification of intracellular ATP:ADP ratio

As described previously,^{19,20} the intracellular ATP:ADP ratio of HUVECs was calculated using fluorescent PercevalHR and pHRed probes. Cells expressing PercevalHR and pHRed probes were imaged using a Zeiss LSM800 inverted confocal microscope with a 40×/1.1 N.A. long working distance water-immersion objective, while a 20×/0.8 N.A. objective was used for time-lapse imaging. Cells were imaged every 10 min for 12 h. An environmental chamber was utilized to keep cells at 37 °C and 5% CO₂. To excite the PercevalHR probe, a 488 and

405 nm laser was used for the ATP-bound and ADP-bound conformation, respectively. Emission was collected through a 450–550 nm band-pass filter. pHRed was excited using a 488 and 405 nm laser, and emission was collected through a 576 nm long-pass filter. After acquiring images, a customized ImageJ macro was used to quantify the normalized ATP:ADP ratio. A mask was generated to outline the cells in each image by merging all channels, subjecting the merged images to a median filter, and converting them to a mask using a Li threshold. The mean background pixel intensity was subtracted from each channel of the images. The mask was applied to images to identify pixels containing fluorescent signals within the cell and calculate the mean pixel intensity of each channel. PercevalHR ratio (F_{488}/F_{405}) and pHRed ratio (F_{488}/F_{405}) were then calculated for individual cells. To correct the pH bias of the PercevalHR probe, we calibrated cells with 15 mM NH₄Cl to alter intracellular pH without altering the intracellular ATP:ADP ratio. The linear correlation between the PercevalHR and pHRed signal was established to predict pH bias in PercevalHR. Only cells in the dynamic range of this linear correlation between the PercevalHR signal and the pHRed signal were included in the study. The PercevalHR ratio was then normalized by dividing the uncorrected PercevalHR signal by the transformed pH-corrected signal.

Quantification of glucose uptake

Glucose uptake was measured using fluorescent glucose analog 2-NBDG (Life Technologies), as described previously.^{19,20} HUVECs in different collagen matrices were incubated in 0.146 mM 2-NBDG for 24 h, then fixed with 3.2% paraformaldehyde (Sigma-Aldrich) in 1× PBS for 15 min at room temperature after washing three times with 1× PBS for 15 min. Z-stack (5 μm slices) images of the entire spheroid were captured using a Zeiss LSM800 confocal microscopy with an excitation laser at 488 nm and emission through a 490–650 nm band-pass filter. To calculate glucose uptake, max z-projection images were generated and subjected to background subtraction, cells were manually outlined, and the mean signal intensity was calculated. The front cell was designated as the tip cell and the cell immediately behind it as the stalk cell. To delineate cell boundaries, cell membranes were labeled with Alexa Fluor 633 conjugated WGA (Life Technologies) for 2 h at room temperature.

Spheroid outgrowth measurement

To measure the outgrowth of HUVEC spheroids embedded in collagen matrices with different concentrations, z-stack (5 μm slices) images of the entire spheroid were captured using a Zeiss LSM800 microscope equipped with a 20×/0.8 N.A. objective. Samples were imaged every 10 min for 12 h in an environmental chamber maintained at 37 °C and 5% CO₂. After capturing time-lapse images, max z-projection images covering the entire area of the spheroids were generated and the length of each sprout and the number of sprouts per spheroid were manually measured using ImageJ (NIH, 2.14.0/1.54f).

Tip–stalk cell rearrangement analysis

To mark each cell and measure tip–stalk cell rearrangement during collective migration, the nuclei of HUVECs in spheroids were labeled with a nuclear dye DRAQ5 (Thermo Fisher). To stain cells with DRAQ5, cells were incubated with 1 μM DRAQ5 in 1× PBS for 1

h at 37 °C and 5% CO₂ and washed twice in 1× PBS for 5 min before generating and embedding spheroids into collagen matrices. DRAQ5-labeled HUVEC spheroids were then imaged using a Zeiss LSM800 confocal microscope with excitation at 640 nm and emission over the 656–700 nm range. A time-lapse imaging was performed to track cell position changes. After capturing time-lapse images, max z-projection images covering the entire area of the spheroids were generated and quantified. Tip–stalk cell exchange was determined based on whether the nucleus of the stalk cell surpassed the tip cell nucleus. The lifetime of tip cells was presented using Kaplan–Meier survival curves, and incomplete observations were used as censored data in the survival analysis. Tip cell lifetime was quantified as the average time a cell remained in the tip position during the 18 h time-lapse. Only multicellular angiogenic sprouts that were stable during the duration of the entire 18 h time-lapse were analyzed for tip cell lifetime, whereas individually disseminated cells and unstable, transient strands that dissociated during the time-lapse were not included in the analysis.

Immunofluorescence staining

Spheroids embedded in collagen matrices of various stiffnesses were fixed in 3.2% paraformaldehyde (Sigma-Aldrich) in 1× PBS for 15 min at room temperature, then washed three times with 1× PBS and permeabilized in 1% Triton X-100 (Sigma-Aldrich) for 1.5 h at room temperature. Samples were then washed for 15 min in 0.02% Tween 20 (Sigma-Aldrich) three times and blocked for 3 h in 1× PBS supplied with 0.02% Tween 20, 10% fetal bovine serum (FBS, Bio-Techne), and 3% bovine serum albumin (BSA; Sigma-Aldrich). Samples were next incubated overnight at 4 °C with rabbit polyclonal CD31/PECAM (1:100; Santa Cruz, sc-1506-R). After three rinses in 0.02% Tween 20 for 2 h each, samples were incubated in anti-goat Alexa Fluor[®] 488 (1:200; Life Technologies) overnight at 4 °C, followed by an additional three, 15 min washes in 0.02% Tween 20. Finally, samples were counter-stained with Alexa Fluor 568 phalloidin (A12380, Life Technology) and 4',6-diamidino-2-phenylindole (DAPI; 1:500; Sigma-Aldrich, D9542).

Confocal reflectance microscopy

Collagen architecture was visualized using a Zeiss LSM800 inverted confocal microscope equipped with a 640 nm laser using a 40×/1.1 N.A. long working distance water-immersion objective and operated by Zen 2.3 software. Pore size and fiber length of each collagen gel was then calculated as previously described.⁴³

Quantitative polarization microscopy

Cell contractility of HUVEC sprouts treated with or without a GLUT1 inhibitor was measured with quantitative polarization microscopy (qPOL) as described previously.²⁴ Images were acquired using a 20×/0.5 N.A. polarization objective with 10° intervals of the polarizer rotation over a range of 0–180°. The polarized image sequences were then processed with a custom MATLAB code to obtain an optical retardance map. The retardance signal proportional to cell contractility was quantified by measuring the average retardance over the area of each sprout after background subtraction.

Western blotting

HUVECs embedded in collagen matrixes with 3 mg/ml or 7 mg/ml concentration were homogenized in Laemmli buffer using the TissueLyserII (Qiagen) and a single 5 mm stainless steel bead (Qiagen). After homogenization, total proteins were extracted with preheated 4× Laemmli buffer and stored at 80 °C until use.⁴⁴ Protein samples were subjected to gel electrophoresis (4%–20% Mini-PROTEAN Precast Protein Gels, BioRad) and western blotting. Membranes were blocked with 5% milk (Millipore Sigma) in TBS. Membranes were then incubated overnight with primary antibodies, anti-glucose transporter GLUT1 antibody (Abcam, ab115730) and anti-β-Actin antibody (Millipore Sigma, A3853), at 4 °C. After incubating with primary antibodies, membranes were then stained with secondary antibodies, IRDye 800CW donkey-anti-rabbit secondary antibody (LI-COR, 926-32213) and IRDye 680RD goat anti-mouse IgG secondary antibody (LI-COR, 926-68070), for 1 h at room temperature. Primary antibodies were prepared at 1:1000 dilution in 5% milk. Secondary antibodies were prepared at 1:2000 dilution. Membranes were imaged using an ImageQuant LAS-4000 system. Quantification was performed with ImageJ (NIH, 2.14.0/1.54f). The relevant protein expression level was expressed as the ratio of the protein of interest to β-Actin.

Statistical analysis

All statistical analyses were conducted using GraphPad Prism 10.0 (GraphPad Software). The D'Agostino–Pearson omnibus normality test was used to check for normality in the spread of data. When comparing two cases, a two-tailed t-test or a two-tailed Mann–Whitney test was used where appropriate. To compare multiple groups, one-way ANOVA or Kruskal–Wallis test with Dunn's post hoc analysis was used. To determine if a curve adequately fit data or to compare two curves, the extra sum-of-squares F-test was used. Pearson's correlation coefficient (*r*) was used to determine correlation. No statistical method was used to predetermine the sample size.

SUPPLEMENTARY MATERIAL

See the [supplementary material](#) for the analysis of Glut1 expression and representative videos of tip-stalk switching in collagen matrixes with varying concentrations.

ACKNOWLEDGMENTS

This work was supported in part by NIH Grant Nos. HL127499 and GM131178 and an award from the W. M. Keck Foundation to C.A.R.-K.; the NCI Predoctoral to Postdoctoral Fellow Transition Award (No. 1F99CA274695) to W.W.; and the NSF Graduate Research Fellowship (Grant No. DGE-1650411) to E. D.F. and M.R.Z. The authors are grateful to Sophie Xie for early analysis of this work.

AUTHOR DECLARATIONS

Conflict of Interest

The authors have no conflicts to disclose.

Ethics Approval

Ethics approval is not required.

Author Contributions

Wenjun Wang: Data curation (lead); Formal analysis (lead); Investigation (lead); Supervision (supporting); Writing – original draft (equal). **Matthew R. Zanotelli:** Conceptualization (equal); Investigation (supporting); Methodology (equal). **Lindsey N. Sabo:** Formal analysis (supporting); Investigation (supporting). **Emily D. Fabiano:** Formal analysis (supporting); Supervision (supporting). **Natalie M. Goldfield:** Formal analysis (supporting). **Chloe Le:** Formal analysis (supporting). **Elle P. Techasiriwan:** Formal analysis (supporting). **Santiago Lopez:** Formal analysis (supporting). **Emily D. Berestesky:** Formal analysis (supporting). **Cynthia A. Reinhart-King:** Conceptualization (equal); Project administration (equal); Resources (equal); Supervision (equal); Validation (equal); Writing – review & editing (equal).

DATA AVAILABILITY

The data that support the findings of this study are available from the corresponding author upon reasonable request.

REFERENCES

- N. Ferrara, “VEGF as a therapeutic target in cancer,” *Oncology* **69**, 11–16 (2005).
- W. Chen *et al.*, “The endothelial tip-stalk cell selection and shuffling during angiogenesis,” *J. Cell Commun. Signaling* **13**, 291–301 (2019).
- R. Blanco and H. Gerhardt, “VEGF and notch in tip and stalk cell selection,” *Cold Spring Harb. Perspect. Med.* **3**, a006569 (2013).
- J. Flournoy, S. Ashkanani, and Y. Chen, “Mechanical regulation of signal transduction in angiogenesis,” *Front. Cell Dev. Biol.* **10**, 933474 (2022).
- Z. Huang and S.-D. Bao, “Roles of main pro-and anti-angiogenic factors in tumor angiogenesis,” *World J. Gastroenterol.* **10**, 463 (2004).
- P. Carmeliet and R. K. Jain, “Angiogenesis in cancer and other diseases,” *Nature* **407**, 249–257 (2000).
- R. K. Jain, “Antiangiogenesis strategies revisited: From starving tumors to alleviating hypoxia,” *Cancer Cell* **26**, 605–622 (2014).
- R. K. Jain, J. D. Martin, and T. Stylianopoulos, “The role of mechanical forces in tumor growth and therapy,” *Annu. Rev. Biomed. Eng.* **16**, 321–346 (2014).
- J. Jakobsson *et al.*, “Endothelial cells dynamically compete for the tip cell position during angiogenic sprouting,” *Nat. Cell Biol.* **12**, 943–953 (2010).
- B. Cruys *et al.*, “Glycolytic regulation of cell rearrangement in angiogenesis,” *Nat. Commun.* **7**, 12240 (2016).
- K. De Bock, M. Georgiadou, and P. Carmeliet, “Role of endothelial cell metabolism in vessel sprouting,” *Cell Metab.* **18**, 634–647 (2013).
- A. R. Cantelmo *et al.*, “Inhibition of the glycolytic activator PFKFB3 in endothelium induces tumor vessel normalization, impairs metastasis, and improves chemotherapy,” *Cancer Cell* **30**, 968–985 (2016).
- F. Bordeleau *et al.*, “Matrix stiffening promotes a tumor vasculature phenotype,” *Proc. Natl. Acad. Sci. U. S. A.* **114**, 492–497 (2017).
- M. Heiss *et al.*, “Endothelial cell spheroids as a versatile tool to study angiogenesis in vitro,” *FASEB J.* **29**, 3076–3084 (2015).
- L. Pfisterer and T. Korff, “Spheroid-based in vitro angiogenesis model,” *Methods Mol. Biol.* **1430**, 167–177 (2016).
- F. Tetzlaff and A. Fischer, “Human endothelial cell spheroid-based sprouting angiogenesis assay in collagen,” *Bio Protoc.* **8**, e2995 (2018).
- M. Potente and P. Carmeliet, “The link between angiogenesis and endothelial metabolism,” *Annu. Rev. Physiol.* **79**, 43–66 (2017).
- M. Tantama, J. R. Martínez-François, R. Mongeon, and G. Yellen, “Imaging energy status in live cells with a fluorescent biosensor of the intracellular ATP-to-ADP ratio,” *Nat. Commun.* **4**, 2550 (2013).
- M. R. Zanotelli *et al.*, “Regulation of ATP utilization during metastatic cell migration by collagen architecture,” *Mol. Biol. Cell* **29**, 1–9 (2018).
- M. R. Zanotelli *et al.*, “Energetic costs regulated by cell mechanics and confinement are predictive of migration path during decision-making,” *Nat. Commun.* **10**, 4185 (2019).
- M. R. Zanotelli *et al.*, “Highly motile cells are metabolically responsive to collagen density,” *Proc. Natl. Acad. Sci. U. S. A.* **119**, e2114672119 (2022).
- J. Zhang *et al.*, “Energetic regulation of coordinated leader-follower dynamics during collective invasion of breast cancer cells,” *Proc. Natl. Acad. Sci. U. S. A.* **116**, 7867–7872 (2019).
- P. Pandya, J. L. Orgaz, and V. Sanz-Moreno, “Actomyosin contractility and collective migration: May the force be with you,” *Curr. Opin. Cell Biol.* **48**, 87–96 (2017).
- W. Wang, J. P. Miller, S. C. Pannullo, C. A. Reinhart-King, and F. Bordeleau, “Quantitative assessment of cell contractility using polarized light microscopy,” *J. Biophotonics* **11**, e201800008 (2018).
- S. P. Carey *et al.*, “Local extracellular matrix alignment directs cellular protrusion dynamics and migration through Rac1 and FAK,” *Integr. Biol.* **8**, 821–835 (2016).
- S. P. Carey, C. M. Kraning-Rush, R. M. Williams, and C. A. Reinhart-King, “Biophysical control of invasive tumor cell behavior by extracellular matrix microarchitecture,” *Biomaterials* **33**, 4157–4165 (2012).
- R. J. Gillies, I. Robey, and R. A. Gatenby, “Causes and consequences of increased glucose metabolism of cancers,” *J. Nucl. Med.* **49**(Suppl. 2), 24S–42S (2008).
- L. Liu *et al.*, “Minimization of thermodynamic costs in cancer cell invasion,” *Proc. Natl. Acad. Sci.* **110**, 1686–1691 (2013).
- B. Cunniff, A. J. McKenzie, N. H. Heintz, and A. K. Howe, “AMPK activity regulates trafficking of mitochondria to the leading edge during cell migration and matrix invasion,” *Mol. Biol. Cell* **27**, 2662–2674 (2016).
- M.-H. Schuler *et al.*, “Miro1-mediated mitochondrial positioning shapes intracellular energy gradients required for cell migration,” *Mol. Biol. Cell* **28**, 2159–2169 (2017).
- P. Bursac *et al.*, “Cytoskeletal remodelling and slow dynamics in the living cell,” *Nat. Mater.* **4**, 557–561 (2005).
- H. Gerhardt *et al.*, “VEGF guides angiogenic sprouting utilizing endothelial tip cell filopodia,” *J. Cell Biol.* **161**, 1163–1177 (2003).
- G. Thurston, I. Noguera-Troise, and G. D. Yancopoulos, “The Delta paradox: DLL4 blockade leads to more tumour vessels but less tumour growth,” *Nat. Rev. Cancer* **7**, 327–331 (2007).
- F. Polet and O. Feron, “Endothelial cell metabolism and tumour angiogenesis: Glucose and glutamine as essential fuels and lactate as the driving force,” *J. Intern. Med.* **273**, 156–165 (2013).
- G. Eelen, P. De Zeeuw, M. Simons, and P. Carmeliet, “Endothelial cell metabolism in normal and diseased vasculature,” *Circ. Res.* **116**, 1231–1244 (2015).
- A. Zecchin, G. Borgers, and P. Carmeliet, “Endothelial cells and cancer cells: Metabolic partners in crime?,” *Curr. Opin. Hematol.* **22**, 234–242 (2015).
- J. Welti, S. Loges, S. Dimmeler, and P. Carmeliet, “Recent molecular discoveries in angiogenesis and antiangiogenic therapies in cancer,” *J. Clin. Invest.* **123**, 3190–3200 (2013).
- M. Potente, H. Gerhardt, and P. Carmeliet, “Basic and therapeutic aspects of angiogenesis,” *Cell* **146**, 873–887 (2011).
- G. Bergers and D. Hanahan, “Modes of resistance to anti-angiogenic therapy,” *Nat. Rev. Cancer* **8**, 592–603 (2008).
- D. Verdegem, S. Moens, P. Stapor, and P. Carmeliet, “Endothelial cell metabolism: Parallels and divergences with cancer cell metabolism,” *Cancer Metab.* **2**, 1–19 (2014).
- M. Martin, A. Veloso, J. Wu, E. A. Katrukha, and A. Akhmanova, “Control of endothelial cell polarity and sprouting angiogenesis by non-centrosomal microtubules,” *eLife* **7**, e33864 (2018).
- A. A. Mamun, H. Hayashi, A. Yamamura, M. J. Nayeem, and M. Sato, “Hypoxia induces the translocation of glucose transporter 1 to the plasma membrane in vascular endothelial cells,” *J. Physiol. Sci.* **70**, 44 (2020).
- P. V. Taufalele, J. A. Vanderburgh, A. Munoz, M. R. Zanotelli, and C. A. Reinhart-King, “Fiber alignment drives changes in architectural and mechanical features in collagen matrices,” *PLoS One* **14**, e0216537 (2019).
- W. Wang *et al.*, “Matrix stiffness regulates tumor cell intravasation through expression and ESRP1-mediated alternative splicing of MENA,” *Cell Rep.* **42**, 112338 (2023).